A VERY EFFICIENT TOOL FOR THE STRUCTURAL ANALYSIS OF HYPERSONIC VEHICLES UNDER HIGH TEMPERATURE ASPECTS

M. HAUPT, H. KOSSIRA, M. KRACHT, J. PLEITNER

Institut für Flugzeugbau und Leichtbau (IFL)
Technische Universität Braunschweig, Deutschland

Institute for Aircraft Design and Structural Mechanics
Technical University Braunschweig, Germany

ABSTRACT

This paper presents a Finite Element Tool, which has been adapted to the requirements of integrated thermal and mechanical analysis of structures. Thus, nonlinear and instationary heattransfer as well as nonlinearities of the mechanical system are considered. The associated basic equations are given. To increase the efficiency of this finite element approach, adaptive grids and sophisticated linear and nonlinear solution algorithms are used. The general strategy is briefly outlined. Examples of instationary and nonlinear problems with special respect to mechanically and aerothermally loaded structures demonstrate the capabilities of the Finite Element Tool.

INTRODUCTION

The structure of vehicles cruising at hypersonic speed is not only exposed to mechanical loads but also to intensive aerodynamic heating. Apart from the selection of materials, which withstand such temperatures, the main interest is foccused on determination of additional thermal-mechanical loadings by reasons of thermal stresses or degradation of material properties leading to a significantly reduced structural performance. Thus, the knowledge of the thermal state becomes essential for the structural analysis, which therefore includes the computation of heattransfer with respect to conduction, convection and radiation. Especially at high temperatures, radiation is one of the main heattransfer phenomena. In the mechanical part, this paper concentrates on thermal stresses resulting from an increasing temperatures as well as temperature gradients combined with a mechanical analysis considering nonlinear deformations and buckling. The structural design requires efficient tools for the multidisciplinary task : an integrated thermal and mechanical analysis [1].

INTEGRATED THERMAL-STRUCTURAL ANALYSIS

Traditionally, an aerodynamicist assumes a rigid isothermal or adiabatic body in order to predict the surface pressure and heating rate. The aerodynamic heating rate is used to compute the temperature distribution inside the structure by a heat transfer analyst. The structural engineer uses temperature distributions and aerodynamic pressures as inputs to predict the structural deformations and stresses. Such an independent approach requires several iteration loops between the different analysis methods and is therefore relativly inefficient as the incompatible mathematical models require extensive postprocessing for data transfer. Moreover, the interdisciplinary couplings and interactions are difficult to handle, because the iterative process calls not only for several additional solutions, but also for remodelling in each analysis.

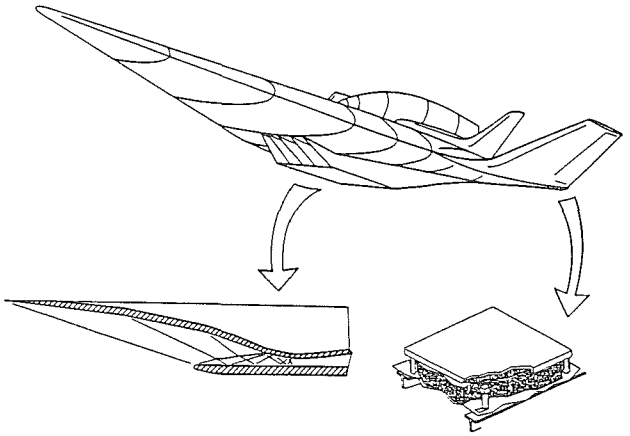

Fig. 1: The structural problems in hypersonic airplane design

To avoid these disadvantanges, an integrated thermal structural analysis is inevitable. *Integrated thermal-structural analysis* means the efficient analysis of coupled thermal and mechanical problems with *one* tool. The simultaneous handling of the thermal and structural problem with one computer-code eliminates not only the restrictions, additional computations and complex data-exchange procedures of the traditional methods, but allows the application of advanced analysis strategies with wellsuited methods for different aspects with significant reduction of computational effort at a desired high accuracy.

In case of a Finite Element Procedure the use of the same grid for the thermal and mechanical analysis heavily redu-

ces the modelling effort, but requires also compatible finite elements, that means elements with similar meshing qualities. Such a *unified* modelling method guarantees the compatibility between the thermal and the structural model and a straightforward data transfer during the coupling of the different physical systems.

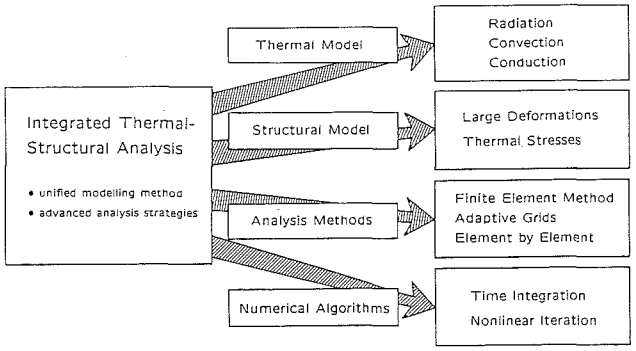

Fig. 2: The strategy of an integrated thermal structural analysis

BASIC EQUATIONS

THERMAL MODEL

The 3D formulation of the thermal model is based on the energy equation, which is in general transient in time. The strong form of this initial-boundary value problem for the temperature distribution Θ with the initial state $\Theta_0 = \Theta(t = t_0)$ consists of the differential equation in the domain Ω

$$\rho c\, \dot{\Theta} + q^i_{,i} = f \tag{1}$$

and of the essential and natural boundary conditions on the boundary Γ

$$\begin{aligned} \Theta - \bar{\Theta} &= 0 \qquad \text{on } \Gamma_\Theta \,, \\ -q^i n_i - \bar{q}_n &= 0 \qquad \text{on } \Gamma_q \,. \end{aligned} \tag{2}$$

The dot indicates the time derivative, $q^i_{,i}$ represents the spacial derivative of the local heatfluxes, f the heat generation per volume. The product ρc - the heat capacity - can be temperature and time dependent, as well as the tensor of heat conductivity κ^{ij}. This tensor is symmetric and provides a linearized relation between the heatfluxes q^i and the temperature gradients $\Theta_{,j}$, which is known as the Fourier law :

$$q^i = -\kappa^{ij}\, \Theta_{,j} \,. \tag{3}$$

Looking on the prescribed heatflux across the boundary $\bar{q}_n$ in detail, the subdivision into three parts is useful :

$$\bar{q}_n = \bar{q}_e + \bar{q}_c + \bar{q}_r \,. \tag{4}$$

The heatflux $\bar{q}_e$ is explicitly given, while $\bar{q}_c$ and $\bar{q}_r$ describe the heatflux by convection and radiation on a free surface. The formulations for these heat transfer phenomenas include the difference between the surface temperature Θ_s and the enviromental temperature $\bar{\Theta}_\infty$:

$$\begin{aligned} \bar{q}_c &= k_c\,(\,\Theta_s - \bar{\Theta}_\infty\,) \,, \\ \bar{q}_r &= k_r\,(\,\Theta_s - \bar{\Theta}_\infty\,) \\ &\qquad \text{with } k_r = \sigma_r \epsilon \psi (\Theta_s + \bar{\Theta}_\infty)(\Theta_s^2 + \bar{\Theta}_\infty^2) \,. \end{aligned} \tag{5}$$

Additionally, the coefficient of convection k_c, the emissivity ϵ, the view factor ψ and the constant of radiation σ_r are to observe. The handling of the radiation is difficult, because strong nonlinearities originating from temperature to the power of three in the generalized radiation coefficient k_r.

With regard to the semidiscretisation – this means the discretisation in space only – the equations of heat transfer can be rewritten in the weak form with the weightened function w

$$\begin{aligned} &\int_\Omega w \rho c \dot{\Theta} d\Omega + \int_\Omega w_{,i} k^{ij} \Theta_{,j} d\Omega \\ &\qquad = \int_\Omega w f d\Omega + \int_{\Gamma_q} w \bar{q}_n d\Omega \,. \end{aligned} \tag{6}$$

Investigations of shell structures make it useful, to modify the basic equations, describing the equations of such a 3D structure with respect to an 2D reference plane (Fig.3). In

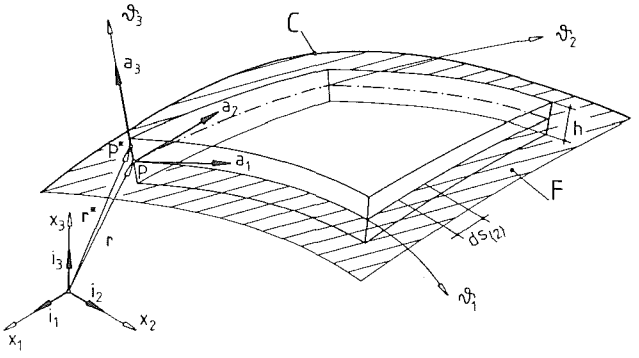

Fig. 3: Geometric description of shells

general, this can be done choosing a set of functions w_i for the weak formulation (6), which are only ϑ^3 dependent. For shell structures a heuristic choice is

$$w_i = (\vartheta^3)^i \quad , \quad i = 0, ..., n \tag{7}$$

and the resulting set of differential equations looks as simple as (1) :

$$^l(\rho c \dot{\Theta}) - {}^l q + {}^l q^\alpha|_\alpha = {}^l f \,. \tag{8}$$

In this approach $^l(\rho c \dot{\Theta})$, $^l q$ and $^l q^\alpha$ are defined by

$$\begin{aligned} {}^l(\rho c \dot{\Theta}) &= \int_{\vartheta^3} \rho c \dot{\Theta}\, (\vartheta^3)^l\, \mu\, d\vartheta^3 \\ {}^l q^\alpha &= \int_{\vartheta^3} q^\alpha\, (\vartheta^3)^l\, \mu\, d\vartheta^3 \\ {}^l q &= \int_{\vartheta^3} q^3\, (\vartheta^3)^{l-1}\, l\, \mu\, d\vartheta^3 \quad , \; {}^0 q = 0 \\ &\qquad l = 1, ..., n \end{aligned} \tag{9}$$

and represents *'moments' of internal energy* and *'moments' of heatflux* up to order l. The loadterm

$$(10) \qquad {}^{l}f = \int_{\vartheta^3} f\,(\vartheta^3)^l\,\mu\,d\vartheta^3 - [\bar{q}_n\,(\vartheta^3)^l\,\mu\,\sqrt{g^{33}}]_{\vartheta_l^3}^{\vartheta_u^3}$$

includes the prescribed heatflux on the upper and lower shell surface with the coordinates ϑ_u^3 and ϑ_l^3. For the transformation of integrals over ϑ^3 the determinant of the metric $g_{\alpha\beta}$ in any point of the shell is shifted by $\mu = \sqrt{g/a}$ into the metric $a_{\alpha\beta}$ of the reference plane. The weak formulation of this description

$$(11) \qquad \begin{aligned} &\int_F w^l(\rho c\dot{\Theta})\,dF - \int_F w^l q - w_{,\alpha}{}^l q^\alpha\,dF \\ &\qquad = \int_F w^l \bar{f}\,dF + \int_{C_q} w^l \bar{q}^\alpha n_\alpha\,ds\ . \end{aligned}$$

includes the thermal loads by heatflux across the boundary curve C. Approximating the temperature in thickness direction with

$$(12) \qquad \Theta(\vartheta^3) = \Theta_0 + \Theta_1\vartheta + ... + \Theta_k(\vartheta^3)^k$$

and using the Fourier law, the constitutive relations are gained :

(13)

$$\begin{aligned} {}^{l}q^\alpha &= \int_{\vartheta^3} q^\alpha(\vartheta^3)^l\,\mu\,d\vartheta^3 = -\int_{\vartheta^3} \kappa^{\alpha\beta}\,(\vartheta^3)^{k+l}\,\mu\,d\vartheta^3\ \Theta_{k,\beta} \\ &\quad - \int_{\vartheta^3} \kappa^{\alpha 3} k(\vartheta^3)^{k+l-1}\mu d\vartheta^3\ \Theta_k\ , \\ {}^{l}q &= \int_{\vartheta^3} q^3\,(\vartheta^3)^{l-1}\,l\,\mu d\vartheta^3 \\ &= -\int_{\vartheta^3} \kappa^{3\beta}\,(\vartheta^3)^{k+l-1}\,\mu\,l\,d\vartheta^3\ \Theta_{k,\beta} \\ &\quad - \int_{\vartheta^3} \kappa^{33}\,(\vartheta^3)^{k+l-2}\,k\,l\,\mu\,d\vartheta^3\ \Theta_k\ ,\ {}^{0}q = 0\,. \end{aligned}$$

Using the shifter μ in its exact form, this approch is applicable without any restrictions to the curvature of shells. It should further be mentioned, that κ^{ij} represents the components of the tensor of conduction, which can be calculated from the physical components by using the tensorial relationships.

If the material properties are variable in thickness direction, for example temperature dependent or if it is composite material, the introduction of a layer model makes sence. Assuming material coefficients to be constant in each layer i the integrals of the constitutive relations are converted into sums, such as :

$$(14) \qquad \int_{\vartheta^3} \kappa^{\alpha\beta}(\vartheta^3)^{k+l}d\vartheta^3 = \sum_i \kappa_i^{\alpha\beta}\tfrac{1}{k+l+1}[(\vartheta^3)^{k+l+1}]_{\vartheta_{il}^3}^{\vartheta_{iu}^3}\,.$$

ϑ_{iu}^3 and ϑ_{il}^3 denotes the upper respectively the lower ϑ^3 coordinate of the individual layer. This approach can be interpreted as a lamina theory for heat transfer.

Mechanical Model

The equations of the mechanical model can also be derived from the equation of energy. Assuming a quasi-static mechanical behaviour, the classical geometric nonlinear formulation leads to the two groups of differential equations of equilibrium and strain-displacement [2]:

$$(15) \qquad \begin{aligned} s^{ij} &= \sigma^{ik}(\delta_k^j + u_{,k}^j) = 0\ , \\ \gamma_{ij} &= \tfrac{1}{2}(u_{i,j} + u_{j,i} + u_{k,i}u_{,j}^k)\ . \end{aligned}$$

In the absence of volume forces the Cauchy stress tensor s^{ij} vanishes and the strain tensor of Green-Lagrange γ_{ij} is defined by a nonlinear relation of the spacial derivatives of the displacements u_i. The coupling between the strain tensor and the second Piola-Kirchhoff stress tensor σ^{ij} is established by the constitutive law. Thermal effects are included by the tensor of thermal expansion α_{ij}, respectively its inverse β^{ij}, and the temperature difference $\Delta\Theta$ related to the thermal expansion free state. Then the constitutive relations can be cast in the linearized form

$$(16) \qquad \begin{aligned} \sigma^{ij} &= E^{ijkl}\gamma_{kl} - \beta^{ij}\Delta\Theta\ , \\ \gamma_{ij} &= F_{ijkl}\sigma^{kl} + \alpha_{ij}\Delta\Theta\ , \end{aligned}$$

since in this paper the mechanical properties are assumed temperature independent. E^{ijkl} represents the tensor of stiffness, F_{ijkl} its inverse. Finally the two types of boundary conditions should be mentioned :

$$(17) \qquad \begin{aligned} u_i - \bar{u}_i &= 0 \qquad \text{on } \Gamma_u\ , \\ s^{ij}n_j - \bar{s}^i &= 0 \qquad \text{on } \Gamma_s\ . \end{aligned}$$

Both are parts in the mixed work principle (16), which is used for discretisation. The principle is based on the principle of Hellinger-Reissner, in which displacements and stresses are independent variables. This formulation needs no postprocessing to calculate the stresses, which are interpolated here with the same quality as the displacements. Therefore it has advantages in nonlinear applications.

$$(18) \qquad \begin{aligned} &-\int_\Omega \delta\tfrac{1}{2}[\sigma^{ij}(u_{i,j} + u_{j,i} + u_{k,i}u_{,j}^k)]d\Omega \\ &+\int_\Omega \delta\tfrac{1}{2}[\sigma^{ij}F_{ijkl}\sigma^{kl}]d\Omega + \int_{\Gamma_s} \bar{s}^j\delta u_j d\Gamma \\ &+\int_{\Gamma_u} s^j\delta u_j + (u_j - \bar{u}_j)\delta s^j d\Gamma = 0 \end{aligned}$$

The derivation of the equations for mechanical behaviour of shells can be done analogous to the shell theory for heat-transfer. In this paper the assumptions of the *Kirchhoff-Love* theory with respect to the kinematic state were used. The resulting theory is valid for moderate rotations including the classical lamina theory and thermal expansion effects; for details see [3].

FINITE ELEMENT TOOL FiPPS

The thermal and structural model in combination with fast and stable numerical algorithms is the first step to an integrated thermal-structural analysis. The resulting tool should fulfil the following requirements :

- consistent finite elements for thermal and mechanical analysis
- models of geometric and physical nonlinear behaviour

- fast solution algorithms for linear and nonlinear systems of equations
- solutions with a controlled high accuracy in time and space

With respect to large systems, vectorization has be considered, to achieve the best performance on supercomputers. This was realized using the finite element package FiPPS of the Institut für Flugzeugbau und Leichtbau (IFL). FiPPS was developed in the last decade to conduct different scientific investigations with finite element methods. FiPPS has a shell-structure and consists of a system-kernel with general software, an inner shell containing problem independent finite element software and an outer shell containing finite element software for special problems. The modular concept of FiPPS makes it easy to configure a new finite element tool with the FiPPS modules and specific extensions.

The configuration of the presented integrated thermal-structural analysis is shown in Fig. 4. Nonlinear material models

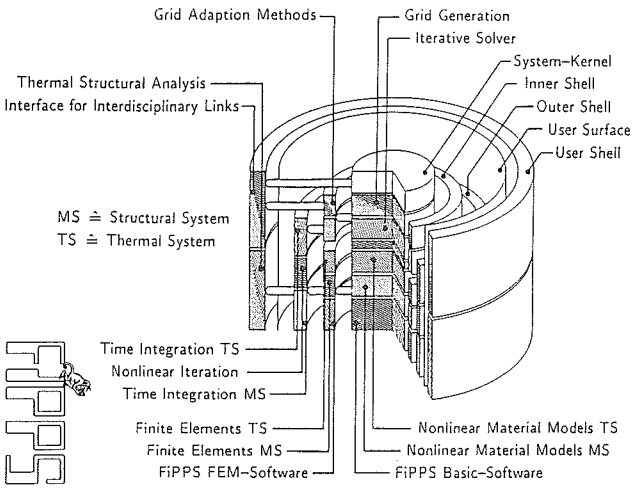

Fig. 4: The finite element program package FiPPS

are located in the system-kernel, the finite element matrices in the inner shell and time integration and iteration algorithms in the outer shell. Furthermore the user-shell is the users's interface for the thermal-structural analysis and represents the interface for interdisciplinary links. The latter is an interface to a Navier-Stokes code, to investigate *fluid-structure interactions.*

FINITE ELEMENTS

Up to now isoparametric finite elements for 2D-problems and shells were implemented. Within the element area the state variables are approximated by means of linear respectively bilinear shapefunctions in a triangle respectively quadrilateral. The choice of such *simple* elements makes it possible to achieve a high vector performance. The mechanical state variables are displacements u_i and stresses $\sigma^{\alpha\beta}$ for 2D-elements or stress resultants for shell elements. In the 2D thermal model the state variable is only the temperature. For the thermal shell element the temperature is approximated in the direction of thickness with a kubic polynom. In this formulation it is possible to fulfil the essential boundary conditions on the lower and upper shell surface better than with linear functions, because the heat-flux is coupled with the temperature gradient, so at least two degrees of freedom are necessary for the gradient. Also for curved shells a nonlinear approximation makes sense. All thermal finite elements include additional terms to the conductivity matrix, which result from the boundary conditions of the convection and radiation type, this has proven benefits in the convergence of such nonlinear problems.

SOLUTION ALGORITHMS

The assembling process of the finite element concept yields the general nonlinear system of ordinary differential equations for the discretisized state $\mathbf{z}$ with time as independent variable :

$$\mathbf{M}\,\dot{\mathbf{z}} + \mathbf{K}\,\mathbf{z} = \mathbf{f}\ . \tag{19}$$

$\mathbf{K}$ represents the matrix of conductivity respectively of stiffness, $\mathbf{M}$ the massmatrix - in this paper present only in thermal problems. The initial state $\mathbf{z_0} = \mathbf{z}(t = t_0)$ completes the problem description. To handle such equations, time integration methods as well as iteration algorithms are components of the finite element tool.

For time integration implicit schemes are prefered, making use of their advantages in stiff problems, which arise for example in the presence of radiation or from very different element sizes as a result of an automatic mesh adaption process. The general scheme of the predictor-corrector method of order $p \leq 1$ consists of two phases. The first phase uses the previously computed results at time t - these are the nodal temperatures and time derivatives up to order p stored in the hypervector $\mathbf{v}$

$$^{t+\Delta t}\mathbf{v} = {}^{t+\Delta t}\left[\mathbf{z}, \Delta t\dot{\mathbf{z}}, ..., \frac{\Delta t^p}{p!}\mathbf{z}^{(p)}\right]^T \tag{20}$$

- to predict the state at $t + \Delta t$:

$$^{t+\Delta t}\mathbf{v}^{(0)} = \mathbf{A}\ {}^{t}\mathbf{z}\ . \tag{21}$$

Matrix $\mathbf{A}$ is the Pascal triangle matrix. The second phase then corrects successively, until convergence is achieved by satisfying the differential equation system.

$$^{t+\Delta t}\mathbf{v}^{(i)} = {}^{t+\Delta t}\mathbf{v}^{(i-1)} + \mathbf{L}_p\ \Delta\mathbf{z}^{(i)} \tag{22}$$

In the correction term, the matrix $\mathbf{L}_p$ is the matrix of relevant integration coefficients. The calculation of the incremental solution vector $\Delta\mathbf{z}$ is carried out with Newton-like methods. In connection with direct solution scheme for linear systems quasi-Newton methods are used, which perform a modification of the iteration-matrix by an updating procedure, Davidon-Fletcher-Powell- (DFP) and Broyden--Fletcher-Goldfarb-Shanno-updates (BFGS), to avoid the costly reformation and inversion of the iteration-matrix. Another approach is the use of Secant-Newton methods first presented by Crisfield, which can be considered as me-

moryless single cycle versions of the DFP and BFGS formulas. Scaled error estimates for neighboured integration orders determine the optimal step-size and order for the next timestep.

Direct elimination methods are limited by storage and computational time, which are increasing superlinear with the number of equations. Furthermore, mesh adaption methods generate new nodes, which can blow up the storage of the systemmatrix, if no expensive renumbering of nodes is performed. Therefore, the idea of the alternative to the direct solvers namely the iterative technique was followed. Of major interest are conjugate gradient (cg) methods with an element-by-element (EBE) preconditioning technique. The preconditioned cg-method includes the system with the preconditioner matrix $\mathbf{P}$. $\mathbf{P}$ should be a good estimate of the inverted original systemmatrix $\mathbf{A}$, but has to be inverted easily. In the EBE-approach introduced by Winget and Hughes [4] from the representation of $\mathbf{A}$

$$\mathbf{A} = \mathbf{D}^{\frac{1}{2}} \left[\mathbf{I} + \mathbf{D}^{-\frac{1}{2}} (\mathbf{A} - \mathbf{D}) \mathbf{D}^{-\frac{1}{2}} \right] \mathbf{D}^{\frac{1}{2}} \quad \text{with } \mathbf{D} = D(\mathbf{A}) \tag{23}$$

the *one-pass-product* form of $\mathbf{P}$ follows with a product over all element contributions

$$\mathbf{P} = \mathbf{D}^{-\frac{1}{2}} \left[\prod_e \left(\mathbf{I} + \mathbf{D}^{-\frac{1}{2}} [\mathbf{A_e} - \mathbf{D_e}] \mathbf{D}^{-\frac{1}{2}} \right)^{-1} \right] \mathbf{D}^{-\frac{1}{2}}. \tag{24}$$

The nature of this approach, which is based on many seperate element contributions, makes EBE methods ideal for vector processing and there is a great potential for parallel processing. The rate of convergency is highly depends on the ratio of massmatrix to matrix of conductivity and therefore dependent on the timestep size for many time-integration schemes. The following example shows this effect.

Subject is a thermal problem : a square with the dimensions $x_1, x_2 \in [0,1]$ (conductivity $k^{\alpha\alpha} = 20$, capacity $\rho c = 2000$) is cooled down from the inital state $\Theta(x_\alpha) = 1000$ by the boundary condition $\Theta(x_1, 0) = \Theta(0, x_2) = 0$. Meshing was accomplished with 80×80 quadrilateral finite elements with one degree of freedom per node. The calculation was performed with the classical Euler-Backward scheme using a controlled time-stepsize. Fig. 5 contains the total CPU-time – including formation of the matrices and solving the system in every timestep – of the solution up to $t = 11s$ at every time-step, measured on the IBM 3090/600J for the one-pass-EBE preconditioned CG-method in comparison with the Gauß-factorization, for which a subroutine of the highly vectorized ESSL-Library was used. It is obvious, that the cg-approch has benefits with respect to the direct solver, when the time-step sizes are small and as a consequence, the massmatrix dominates over the conductivity matrix. This can be seen at the initial gradient, which is constant for the Gauß-factorization and nearly one half of the cg-method. This is caused by a relativly small number of iterations, which are plotted against the time-step size in Fig. 6. In accordance with increasing time-step size the number of iterations grows up to 38. The decreasing number of iterations behind the maximum is caused

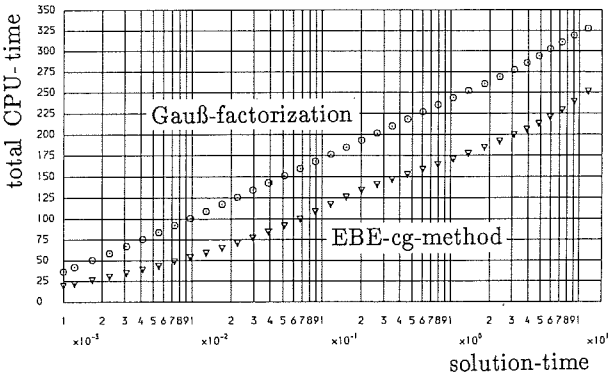

Fig. 5: CPU-times, EBE-cg-method and Gauß-factorization

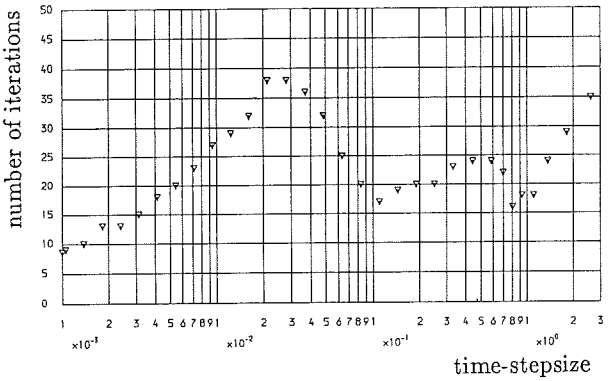

Fig. 6: Number of iterations of the EBE-cg-method

by the activation of an absolute convergence criteria, which finished the iteration, if the temperature increment is lower than $5K$.

ADAPTIVE GRIDS

To increase efficiency and accuracy of the finite element solution, the thermal-mechanical grid is adaptively refined and coarsened. Fig. 7 shows the integration of the grid-adaption method in the time-stepping sequence. After several time-steps an error estimation is carried out for the state, that has been reached. Controlparameters and the calculated error estimations indicate a reiteration of the time-steps with a refined grid or a continuation of the time-stepping with a refined and coarsened grid.

For error estimations, the residuum- and postprocessing methods are applied. Error estimation in thermal analysis with postprocessing methods is done with the Zienkiewicz-Zhu estimation. The results of this estimation technique are proven to be reliable. In the mechanical analysis, the error estimation is derived from the difference of the direct calculated stress-field – assumed to be exact – and the stress-field, calculated indirectly from the differentiated displacements. With respect to refinement and coarsening tolerances, the calculated error estimates determine the elements, which shall be refined or coarsened.

For the examples given in this paper, the classical h-adaption is employed in conjunction with triangular and quadrilateral discretization in two dimensions. In the refinement of an indicated element, only a division into four child-elements is allowed [5]. The new nodes are created on the midpoints of the element sides. Particular in the case of triangles in the transition element layer, triangles are divided into two, to avoid irregular grids. These halves are not allowed to be refined, but the basis element. The local coarsening is possible if the four child-elements are indicated for coarsening. Then the child-elements are deleted and the parent-element is activated. This strategy stores the data of the whole grid hierachy, but is very fast in transient problems, where local grid modifications are performed in a few percents of the computational time.

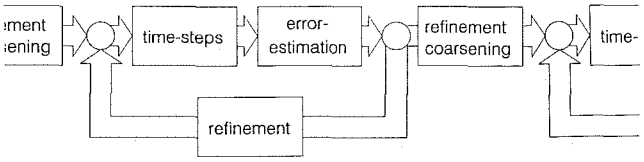

Fig. 7: The grid adaption strategy

NUMERICAL EXAMPLES

Subject of the first examples is a square plate with a geometry depicted in Fig. 8. The material properties are those of fibre reinforced ceramic. Thermal loads come from a uniform heatflux q_0 and additionally from a heat load peak 20 times higher than q_0, which goes along a line slightly rotated against the symmetry line ($x_1 = 0.4x_2 + 75$). The shape of the heatload was assumed as a $(1 + \cos)$ distribution in the cross-section and constant along the line. Such a heatflux peak can be a consequence of an aerodynamic shock and represents a loading causing high temperature gradients. The first set of boundary conditions is shown in Fig. 8. All edges of the plate are kept at $270K$. The upper surface emits heat by radiation, while the lower surface is insulated. It should be emphasized, that in this example the prescribed temperature at the edges of the plate is a very strong condition.

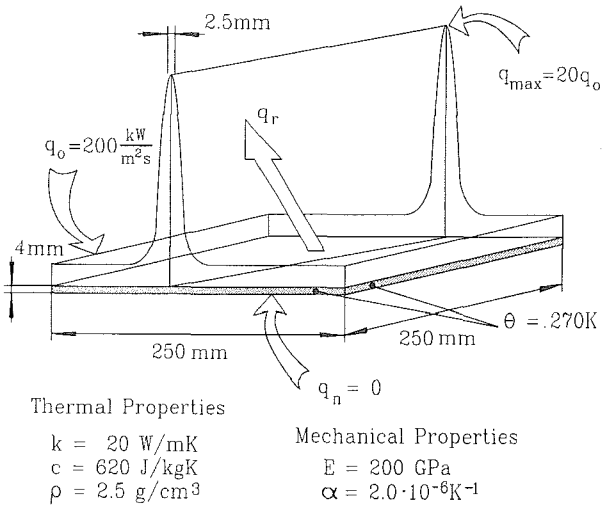

Fig. 8: The geometry and thermal loads of a shock-heated plate

STATIONARY TEMPERATURE DISTRIBUTION IN A CROSS-SECTION

In the first investigation the problem is reduced to two dimensions and the resulting model represents the cross-section at the symmetry line of the plate. Adaptively refined regular triangle-grids are used for idealization. Fig. 9 shows the initial uniform mesh with 303 nodes and the 4 times refined mesh with 817 nodes for the stationary solution of the temperature. Error criteria was the heatflux, which was reduced from 15% up to 4%. The grid adaption process indicates very well the zone, where a fine grid is necessary to calculate the exact solution. In the particular case the refinement is done in the area of the heatload peak, where the inital grid is not able to represent such a temperature distribution, as it can be seen at the isotherms in Fig. 9.

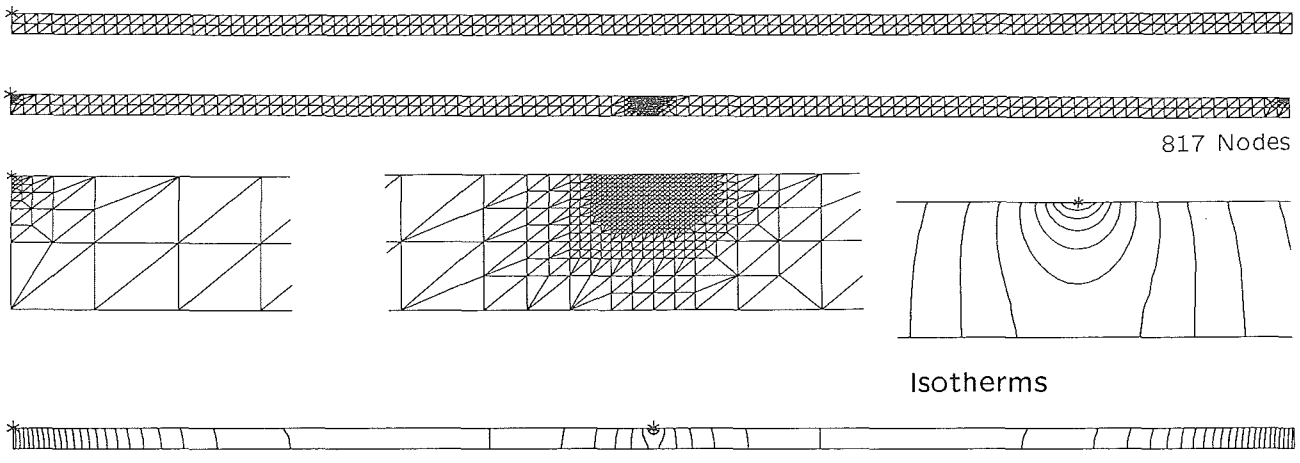

Fig. 9: Solution with adaptive grid refinement

INSTATIONARY TEMPERATURE DISTRIBUTION IN A CROSS-SECTION

To demonstrate the capabilities of the grid adaption strategy, in the second example the shock moves. The movement happens with constant velocity of $7.5\frac{mm}{s}$ from the midpoint of the plate $75mm$ to the right hand side. The calculation was performed with a slightly smaller refinement tolerance as in the stationary analysis, to get the temperature peak within a greater refinement zone. As a consequence of the moving heat peak the temperature follows the heat peak as shown in Fig. 10, where the temperature distribution of the upper surface is plotted against the x_1-axis at different times.

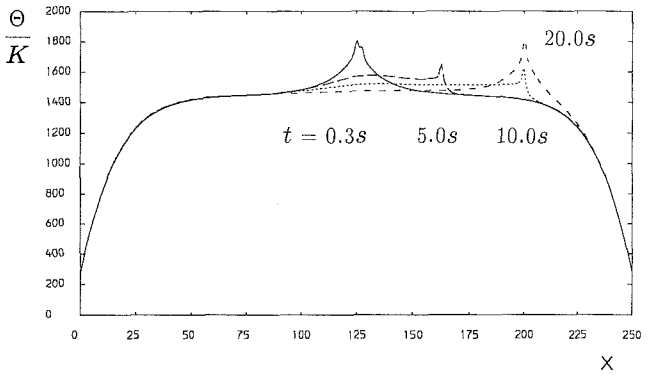

Fig. 10: Transient temperature distribution at the upper plate surface

Fig. 11 shows the corresponding isotherms ($\Delta\Theta = 25K$) and grids belonging to the different time steps :

- at $0.3s$, the moving of the heatload peak is indicated by the eccentricity of the isotherms and in the grid refinement
- at $5s$, induced by the heatcapacity, a zone of higher temperature behind the shock can be recognized as well as a decrease in the maximum temperature. The grid at the initial heat peak position is fully coarsened, and caused by the mesh strategy, local grid refinements of foregoing timesteps forms an unnecessary zone of refinement behind the shock.
- at $10s$, the heat source arrives at its endpoint. The maximum temperature decreases up to $1605K$. Again a temperature and refinement drag can be observed. Up to now, the right area is nearly undisturbed of the moving shock.
- at $20s$, this state can be assumed as the stationary one, where the maximum temperature increases up to $1812K$. The grid adaption strategy eliminates the unnecessary grid refinements of the moving shock

STATIONARY TEMPERATURE DISTRIBUTION OF THE PLATE

Considering the 3D-structures of the whole plate, the following calculations were performed with the thermal shell element. To avoid too much refinement levels in the finite element model, the width of the heatload peak was spread from $2.5mm$ to $5mm$ and the intensity was halved, so the results are comparable with the previous discussed. Starting with a 2×2 finite element grid, the adaption process forms the grid shown in Fig. 12 for the stationary solution. The isotherms belonging to the temperature distribution of the upper and of the lower surface are depicted in Fig. 13.

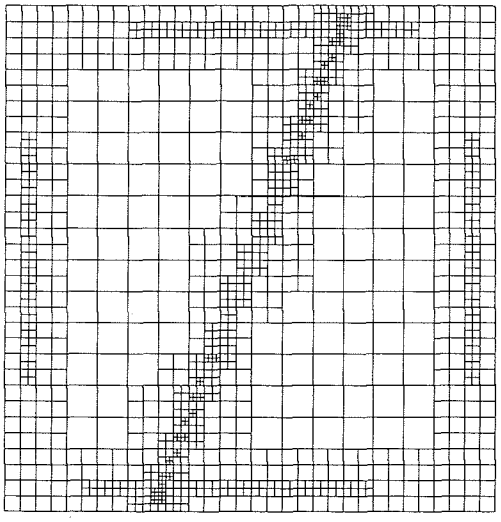

Fig. 12: Adaptively refined grid of the plate

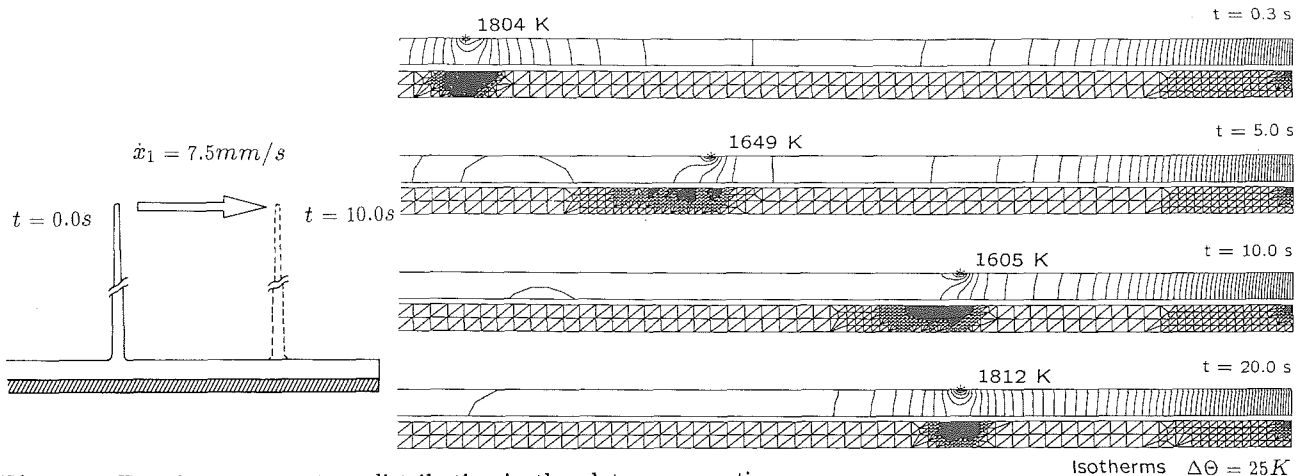

Fig. 11: Transient temperature distribution in the plate cross-section

Significant is the influence of the heatload peak causing a line of maximum temperature, whose amplitude is nearly constant.

Compared with the temperature distribution in the cross-section the isotherms of both plate sides show the same characteristics : sharp gradients at the edges and in the area of the shock. These gradients force a grid refinement and so the solution becomes smooth. The reached maximum temperatures of $1787K$ on the top and $1679K$ on the bottom of the plate are good result, in comparison with the results of the cross-section. In the areas, where the shock cross the plate boundaries, the grid is specially densed, since the temperature distribution is more complex.

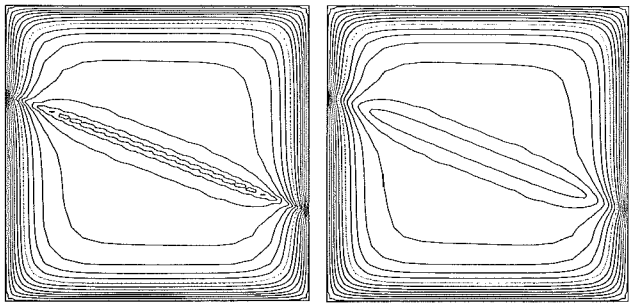

Fig. 13: Temperature distribution at the upper (left) and lower (right) plate surface,
dots : $\Theta = 1000K$, $\Delta\Theta = 100K$

STATIONARY DEFORMATION OF THE PLATE CROSS-SECTION

Now the mechanical analysis as part of the integrated thermal-structural tool will be demonstrated at the 2D cross-section of the plate. The edges of the model were assumed to be clamped and the load consists of a pressure of $p = 0.2N/mm^2$ on the top of the plate and the temperature distribution of the previously discussed stationary solution. The temperature-rise forces a pressure stress σ^{11}, which leads to a nonlinear behaviour : the plate buckles. The angle of deflection increases at its maximum up to 4°, which may influence the aerodynamic flow-field.

It should be mentioned, that in this example the nonlinear analysis is necessary, because buckling produces higher stresses and the material may fail. If a linear calculation is performed, the stress component σ^{11} will increase up to $-270N/mm^2$, but the superposition of the nonlinear deflection results in a maximum pressure stress, which is four times higher. Fig. 14 shows the stress component σ^{11}. It can also be seen, that the disturbance by the local heating is small. As a consequence of the last example, it is necessary to perform a mechanical analysis of the whole plate.

NONLINEAR BEHAVIOUR OF SHELLS

Studies of cylindrical shells made with the mechanical shell element without coupling were carried through. The nonlinear behaviour – that means bending and buckling – is an essential aspect of thin shell structures. The studies were performed with material properties such as carbon reinforced carbon, geometry and material data are depicted in

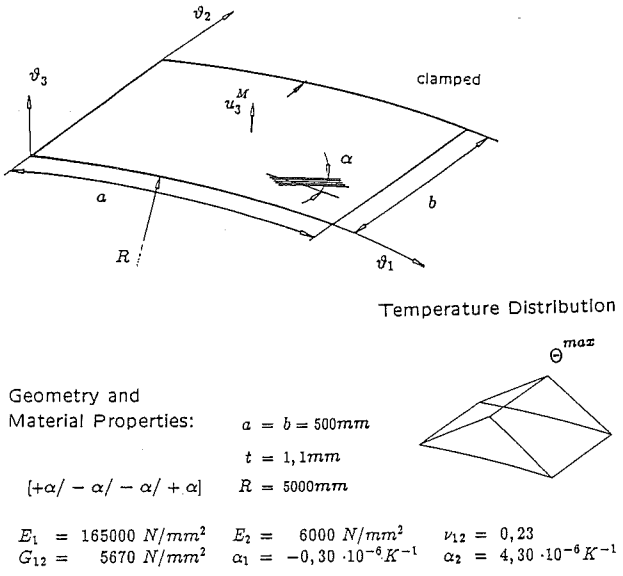

Fig. 15: Geometry and material properties of a cylindrical shell

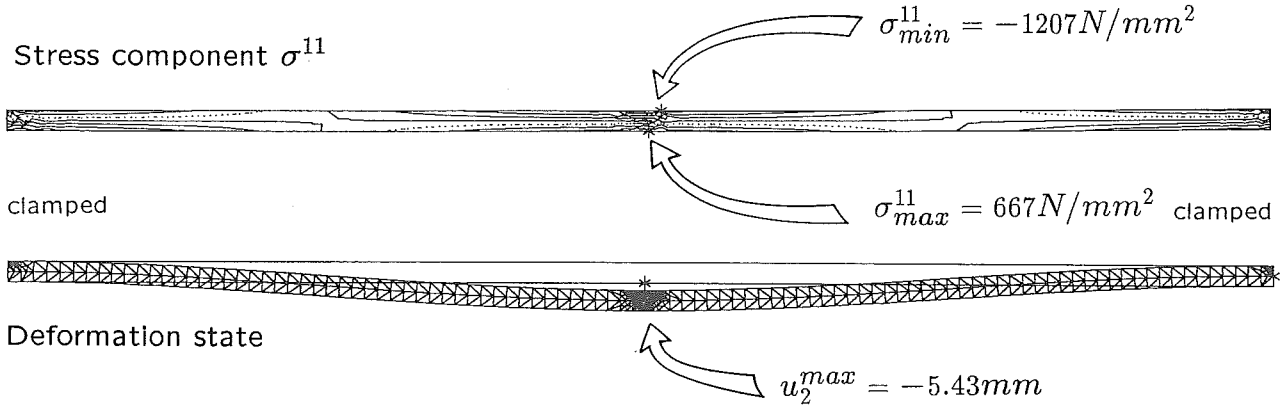

Fig. 14: Nonlinear deformation under thermal loads and stress component σ^{11}

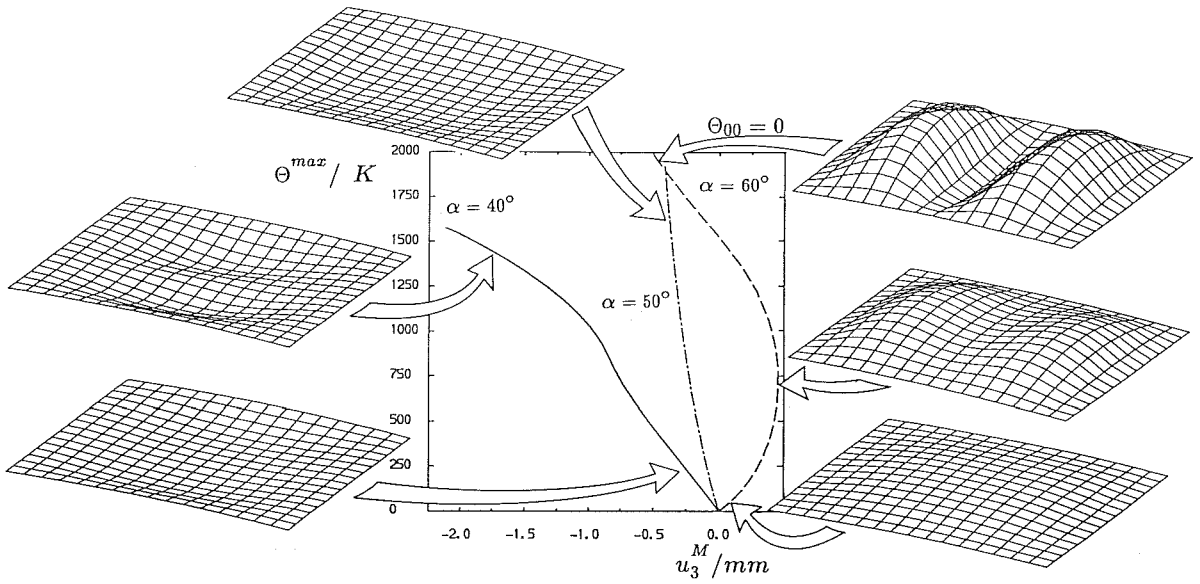

Fig. 16: Nonlinear behaviour of a cylindrical shell under thermal loads

Fig. 15. The temperature is a linear approximation of the shock-induced one.

Fig. 16 shows the nonlinear deflection of the centerpoint of the shell plotted against the maximum temperature for different lamina-orientation-angles α and the corresponding deflection patterns for symmetric laminates. The main buckle-orientation changes within a limited range from the circumferential direction ($\alpha = 40°$) to the meridian direction ($\alpha = 60°$). Details of this investigations are presented in [6]

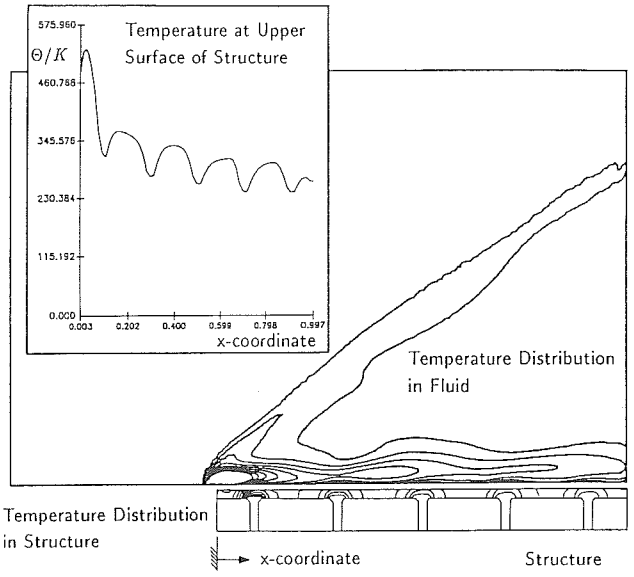

Fig. 17: Temperature solution of a computed fluid-structure interaction

FLUID STRUCTURE INTERACTION

An essential aspect in investigations of hypersonic vehicles is the determination of the heatflux into the structure, which depends on the aerodynamic flow-field. The aerodynamic flow field itself is influenced by the thermal and mechanical response of the structure. If such strong fluid-structure interactions occur, for example in the stationary case, the appearance of hot spots or in the dynamic case, panel flutter, an integrated fluid-thermal-structure analysis is necessary. To make such investigations the thermal mechanical tool FiPPS was extended with an interface to the finite element navier-stokes code of the Institut für Strömungsmechanik of the Technical University Braunschweig.

Subject of the example shown in Fig. 17 is a stiffened plate with parallel hypersonic flow, which causes a temperature maximum at the plate tip. The boundary layer is obviously altered by the stiffeners, acting as heatsinks. The aim of this testcase, to demonstrate the coupling of the computer codes, was successfully reached.

CONCLUDING REMARKS

The structural design of hypersonic vehicles makes efficient analysis tools necessary, including interdisciplinary aspects. The concept and realization of an integrated thermal-structural analysis tool is described in this paper. It combines methods for thermal and mechanical modelling based on finite element methods. An effective solution is possible, using powerful finte elements in connection with sophisticated algorithms, like grid adaption. With respect to large systems of equations and strong nonlinearities, modern linear and nonlinear solution techniques as well as special time integration schemes have to be parts of such a tool. The tool

was configurated out of the finite element package FiPPS. The presented examples show the functionality of the code in solving thermal-mechanical problems at high temperatures. It could be demonstrated, that the tool handles nonlinearities and local effects with its fast solution- and grid-algorithms in a very efficient way. Furthermore, for coupled fluid thermal structural analysis in cases of strong fluid-structure interactions the tool can be interfaced to a navier-stokes code. The way realizing such a tool is proven to be successful and will be pursued.

ACKNOWLEDGEMENT

The authors gratefully acknowledge the financial support of their investigations by the Deutsche Forschungsgemeinschaft (Sonderforschnungsbereich 257).

REFERENCES

[1] WIETING, A.R.; DECHAUMPHAI, P.; BEY, K.S.; THORNTON, E.A.; MORGAN, K. : Application of Integrated Fluid-Thermal-Structural Analysis Methods; Thin-Walled Structures **11**, 1991, 1–23

[2] HETNARSKI, R.B. : Thermal Stresses I; North-Holland; Amsterdam, New York, Oxford, Tokyo; 1986

[3] WOLF, K. : Untersuchungen zum Beul- und Nachbeulverhalten schubbeanspruchter Teilschalen aus kohlefaserverstärktem Kunststoff; Ph.D.Thesis; TU Braunschweig, 1988

[4] WINGET, M., HUGHES, H. : Solution algorithms for nonlinear transient heat conduction analysis employing element-by-element iterative strategies, Comp. Meths. Appl. Mech. Engrg. **52**, 1985, 711–815

[5] LÖHNER, R. : An Adaptive Finite Element Scheme for Transient Problems in CFD; Comput. Meths. Appl. Mech. Engrg. **61**, 1987, 323–338

[6] KOSSIRA, H.; HAUPT, M. : Buckling of Laminated Plates and Cylindrical Shells Subjected to Combined Thermal and Mechanical Loads, in: Proc. of the Int. ECCS-Colloquium : On the Buckling of Shell Structures on Land, in the Sea and in the Air, Lyon, 1991, to appear